Desert seismic data denoising based on energy spectrum analysis in empirical curvelet domain

MO LI, YUE LI✉, NING WU AND YANAN TIAN

College of Communication and Engineering, Jilin University, Jilin 132000, China
(liyue@jlu.edu.cn)

Received: October 11, 2019; Revised: January 7, 2020; Accepted: April 15, 2020

ABSTRACT

Desert seismic events are disturbed and contaminated by strong random noise, which complicates the subsequent processing, inversion, and interpretation of the data. Thus, noise suppression is an important task. The complex characteristics of random noise in desert seismic records differ completely from those of Gaussian white noise such that they are non-stationary, non-Gaussian, non-linear and low frequency. In addition, desert seismic signals and strong random noise generally share the same frequency bands. Such factors bring great difficulties in the processing and interpretation of desert seismic data. To obtain high-quality data in desert seismic exploration, we have developed an effective denoising method for desert seismic data, which performs energy spectrum analysis in the empirical curvelet transform (ECT) domain. The empirical curvelet coefficients are divided into two different groups according to their energy spectrum distributions. In the first group, which contains fewer effective signals, a large threshold is selected to remove lots of random noise; the second group, with more effective signals, a coherence-enhancing diffusion filter (CEDF) is used to eliminate the noise. Unlike traditional curvelet transforms, ECT not only has the multi-scale, multi-direction, and anisotropy properties of conventional curvelet transform, but also provides adaptability to separate the effective signals from the random noise. We examine synthetic and field desert seismic data. The denoising results demonstrate that the proposed method can be used for preserving effective signals and removing random noise.

Keywords: empirical curvelet transform, desert seismic random noise, energy spectrum, coherence-enhancing diffusion filtering, CEDF, denoising

1. INTRODUCTION

The worldwide demand for oil, natural gas, and other energy resources has become a major challenge. Seismic exploration is vital for accessing such resources. Because easily obtainable exploration and exploitation resources are becoming exhausted, research has shifted to deep, thin layers and complex geological structures underground. The Tarim Desert Basin in western China is rich in oil and gas resources. However, harsh

environment and complex surface conditions cause strong random noise in the collected seismic data, which seriously affects identification of the effective information. Unlike mountain land, forest belts, and other regions, the sand layer in the desert region is loose. This leads to the stronger energy of desert seismic noise. Additionally, because this loose sand absorbs most of the high-frequency noise, desert seismic noise is mainly characterized by low-frequency. The resulting difficulty in suppressing desert seismic random noise is greatly increased (more details in *Li and Li, 2016*; *Li et al., 2017*); therefore, improving the signal-to-noise ratio (*SNR*) of desert seismic data is important for the processing work.

During the last few decades, many methods have been applied to suppress random noise in seismic signal processing such as frequency-wave number (*f-k*) filter (*Naghizadeh, 2012*), non-local mean filter (*Bonar and Sacchi, 2012*), adaptive filtering (*Ristau and Moon, 2001*; *Jeng et al., 2009*), empirical modal decomposition (*Bekara and van der Baan, 2009*), singular value decomposition (*Deng et al., 2008*), Bayesian inversion (*Yuan and Wang, 2013*), etc. These algorithms combined with other methods have been used for improving their drawbacks in noise suppression of seismic data with good results. Though these methods have been successful in practical applications, they are used mainly for suppressing the white Gaussian noise. In fact, the characteristics of the desert seismic random noise are non-Gaussian, non-stationary, non-linear, low-frequency, which are totally different from random Gaussian noise. Additionally, effective signal and strong random noise of desert seismic data overlapped seriously in frequency domain (*Zhong et al., 2015, 2019*). All these factors cause limitations in the analysis of desert seismic data. Therefore, a new method is critical for effectively suppressing the desert seismic random noise and obviously enhancing the *SNR*.

Wavelet transform (WT) is a classical multi-scale analysis method with good time-frequency localization ability, which has been successfully applied in seismic exploration (*Fu et al., 2015*; *Miao and Moon, 1999*). However, the excellent characteristics of WT in one dimension cannot be generalized to two or more dimensions. WT can effectively approximate only point singularities rather than line singularities, which brings certain limitations in processing complex multidimensional signals.

To overcome such limitations, multiscale geometric analysis has been developed rapidly and applied with satisfactory results in the field of signal processing. In particular, the traditional curvelet transform (TCT) proposed by *Candes et al.(2006)* has been widely used for seismic signal processing(*Gong et al., 2018*) owing to its multi-scale, multi-direction, and anisotropy characteristics.

Neelamani et al. (2008) proposed coherent and random noise attenuation using the curvelet transform. *Herrmann et al. (2004)* proposed a curvelet-domain multiple elimination method with sparseness constraints. *Hennenfent (2010)* proposed a non-equispaced fast discrete curvelet transform for seismic data reconstruction. However, because the traditional curvelet basis function is not adaptive, it no longer meets the denoising accuracy requirement when processing complex desert seismic data.

Given the shortcoming of TCT, *Gilles et al. (2014)* proposed a new adaptive signal processing method, namely, empirical curvelet transform (ECT). The concept of this method is to design an adaptive filter bank according to the information of the signal itself to extract the different modes of the signal, thus obtaining the ECT coefficients for different scales and directions. Applying a threshold on the obtained coefficients is

a classical denoising method reported by *Donoho (1995)*. However, the denoising effect depends on the size of the threshold. An excessively large or small threshold leads to restraining or reserving too many coefficients. In addition, desert seismic random noise possessed the characteristics of low-frequency and large amplitude. Therefore, such methods based on threshold are sub-optimal. In the present study, we propose a method of desert seismic data denoising based on ECT by taking the energy spectrum distribution of the coefficients into account. First, the adaptive filter banks are constructed by empirically detecting the Fourier supports. Then, the ECT coefficients of different components are obtained by filtering the input signal with the obtained filter bank. Subsequently, the empirical curvelet coefficients are divided into two categories based on their energy spectrum distribution. For those associated with noise, we select a large threshold to remove much noise; we perform coherence-enhancing diffusion filter (CEDF) (*Weickert and Scharr, 2002*) on those associated with effective signals. Finally, we used the inverse ECT to reconstruct the coefficients and to obtain the denoising results.

The remainder of this paper is organized as follows. In Section 2, the mathematical theory of ECT is reviewed. Section 3 describes the processing of the ECT coefficients. In Section 4, the validity of our algorithm is tested on the synthetic records and field data. Finally, we give the conclusion in Section 5.

2. PRINCIPLES

2.1. Curvelet transform

We first briefly introduce the TCT. Curvelet transform is a multi-scale and multi-direction transform proposed for solving the problem that the WT cannot effectively approximate the line singularities. Similar to WT, this method uses inner product of basis function and signal to achieve sparse representation of signal.

The curvelet transform is a data function mapping, and the curvelet coefficient $C(j,l,k)$ can be expressed as the inner product of the two-dimensional function *f* and the curvelet basis function $c_{j,l,k}$, that is,

$$C(j,l,k)=\left\langle f, c_{j,l,k}\right\rangle=\int_{R^2} f(x)\overline{c_{j,l,k}(x)}\,dx, \tag{1}$$

where *j*, *l*, *k* denote the scale, direction and position parameter, respectively; $k=(k_1,k_2)$, $k_1, k_2 \in Z$; with *Z* as the set of integers; $\overline{c_{j,l,k}}$ is the complex conjugate of $c_{j,l,k}$. The Fourier transform of one curvelet basis function $c_{j,l,k}$ can be constructed by a window function *U*, and it can be decomposed by scale and angle in the frequency domain. The function U is composed of a pair of smooth, non-negative and real windows, radial window $W(r)$ and angular window $V(t)$. These windows obey the following conditions:

$$\sum_{j=-\infty}^{\infty} W^2\left(2^j r\right)=1, \quad r\in\left(\frac{3}{4},\frac{2}{3}\right), \tag{2}$$

$$\sum_{l=-\infty}^{\infty} W^2\left(t-l\right)=1, \quad t\in\left(-\frac{1}{2},\frac{1}{2}\right). \tag{3}$$

Then, for each $j > j_0$ a window U_j can be expressed in the Fourier domain as:

$$U_j\left(r,\theta\right)=2^{-3j/4}W\left(2^{-j}r\right)V\left(\frac{2^{\lfloor j/2\rfloor}\theta}{2\pi}\right), \tag{4}$$

where t is time, r and θ are the radius and angle, respectively, in the Fourier plane, and $\lfloor j/2\rfloor$ represents the integer part of $j/2$. The support of the U_j is a polar "wedge", as illustrated in the shadow area of Fig. 1a.

The algorithm employs a dyadic decomposition to separate the Fourier plane. The low frequencies are located on a disk centered at zero frequency; each scale is defined on a concentric ring; the angular range corresponding to each angular sector is also split into dyadic intervals, and for fine-scales, their number doubles every other two scales.

2.2. Empirical curvelet transform

The basis function of the TCT is fixed, whereas that of the ECT is adaptive, as shown in Fig. 1b. Because the information differs among the signals, the ECT can decompose the signal to different scales and directions according to the content of the signal itself. In brief, the main idea of the ECT is to extract the different amplitude modulated - frequency modulated (AM-FM) components of a signal by constructing an adaptive filter bank. There are two steps to be performed:

1. Compute the pseudo-polar fast Fourier transform of signal $f\left(x\right)$. Some work has been done on the construction of a pseudo-polar Fourier transform (*Averbuch et*

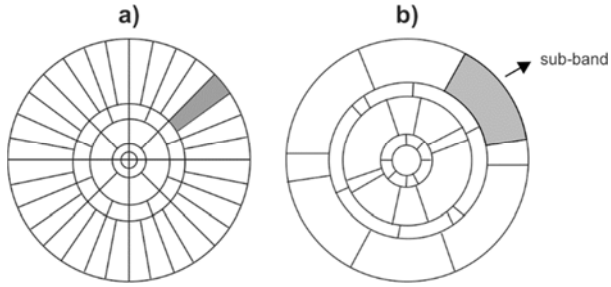

Fig. 1. Curvelet tiling of the Fourier plane: **a)** traditional curvelet transform, **b)** empirical curvelet transform. In the frequency domain, curvelets are supported near a "parabolic" wedge (shadowed area).

al., 2006, 2008). It is assumed that the number of scales N and angular sectors M to be divided are given, then a series of scale boundaries $\Omega_\omega = \left\{\omega^n\right\}$, $n = 0, 1, \ldots, N$, where ω represents the circular frequency, and angle boundaries $\Omega_\theta = \left\{\omega^m\right\}$, $m = 0, 1, \ldots, M$, can be obtained by performing Fourier boundary detection. We consider that detection of the angles Ω_θ depends on the scales Ω_ω. In addition, the local maxima method is adopted to detect the boundary and the details of segmentation method will be introduced in Section 2.3.

2. The corresponding adaptive filter bank $\Phi = \left\{\varphi_1(x), \left\{\psi_{nm}(x)\right\}_{\substack{n=1,\ldots,N-1\\ m=1,\ldots,M}}\right\}$ is constructed by using both the Meyer wavelet and Littlewood-Paley wavelet (*Daubechies, 1992*), where $\varphi_1(x)$ is the low-pass filter located at the centre of the Fourier plane and $\psi_{nm}(x)$ is the polar wedge support in the Fourier domain formed by radial window W_n and polar window V_m. The Fourier transform of $\varphi_1(x)$ is given by

$$\varphi_1(\omega) = \begin{cases} 1 & \text{if} \quad |\omega| \le (1-\gamma)\omega^1, \\ \cos\left(\frac{\pi}{2}\beta\left(\frac{1}{2\gamma\omega^1}\left[|\omega| - (1-\gamma)\omega^1\right]\right)\right) & \text{if} \quad (1-\gamma)\omega^1 \le |\omega| \le (1+\gamma)\omega^1, \\ 0 & \text{otherwise}. \end{cases} \tag{5}$$

The Fourier transform of W_n and V_m are defined as:

$$W_n(\omega) = \begin{cases} 1 & \text{if} \quad (1+\gamma)\omega^n \le |\omega| \le (1-\gamma)\omega^{n+1}, \\ \cos\left(\frac{\pi}{2}\beta\left(\frac{1}{2\gamma\omega^{n+1}}\left[|\omega| - (1-\gamma)\omega^{n+1}\right]\right)\right) & \text{if} \quad (1-\gamma)\omega^{n+1} \le |\omega| \le (1+\gamma)\omega^{n+1}, \\ \sin\left(\frac{\pi}{2}\beta\left(\frac{1}{2\gamma\omega^{n}}\left[|\omega| - (1-\gamma)\omega^{n}\right]\right)\right) & \text{if} \quad (1-\gamma)\omega^{n} \le |\omega| \le (1+\gamma)\omega^{n}, \\ 0 & \text{if} \quad \text{otherwise} \end{cases} \tag{6}$$

for $n \neq N-1$,

$$W_{N-1}(\omega) = \begin{cases} 1 & \text{if} \quad (1+\gamma)\omega^{N-1} \le |\omega|, \\ \sin\left(\frac{\pi}{2}\beta\left(\frac{1}{2\gamma\omega^{N-1}}\left[|\omega| - (1-\gamma)\omega^{N-1}\right]\right)\right) & \text{if} \quad (1-\gamma)\omega^{N-1} \le |\omega| \le (1+\gamma)\omega^{N-1}, \\ 0 & \text{if} \quad \text{otherwise} \end{cases} \tag{7}$$

for $n = N-1$, and

$$V_m(\theta)=\begin{cases}1 & \text{if} \quad \theta^m+\Delta\theta\le\theta\le\theta^{m+1}-\Delta\theta,\\ \cos\left(\frac{\pi}{2}\beta\left(\frac{1}{2\Delta\theta}\left(\theta-\theta^{m+1}+\Delta\theta\right)\right)\right) & \text{if} \quad \theta^{m+1}-\Delta\theta\le\theta\le\theta^{m+1}+\Delta\theta,\\ \sin\left(\frac{\pi}{2}\beta\left(\frac{1}{2\Delta\theta}\left(\theta-\theta^{m}+\Delta\theta\right)\right)\right) & \text{if} \quad \theta^{m}-\Delta\theta\le\theta\le\theta^{m}+\Delta\theta,\\ 0 & \text{if} \quad \text{otherwise},\end{cases} \tag{8}$$

where $\theta^{m-1}=\theta^l+\pi$, ω and θ are the polar coordinates on the Fourier plane, γ is a parameter that ensures no overlap between the two consecutive transitions usually belongs to (0, 1). The function $\beta(x)$ is an arbitrary function that satisfies the following properties:

$$\beta(x)=\begin{cases}0 & \text{if} \quad x\le 0,\\ \beta(x)+\beta(1-x)=1 & \text{if} \quad x\in(0,1),\\ 1 & \text{if} \quad x\ge 1.\end{cases} \tag{9}$$

Thus, the ECT coefficients can be expressed as:

$$Coe(n,m)=\langle f(x),\Phi\rangle=\int f(x)\Phi\,dx. \tag{10}$$

The inverse transform is obtained by:

$$f(x)=Coe(0)*\phi_0(x)+\sum_{n=1}^{N-1}\sum_{m=1}^{M}Coe(n,m)*\psi_{nm}(x), \tag{11}$$

where * denotes convolution product.

2.3. Segmentation of the Fourier spectrum

The method of dividing the Fourier spectrum is critical because it is the step to find the Fourier support used to build the filters. There are several segmentation methods to be used in ECT, such as locmax, locmaxmin, locmaxminf, and scale-space. The locmax is a simple and easily understood method for detecting the set of Fourier boundaries, based on the computation of local maxima with the boundaries set as midpoints between consecutive maxima. Therefore, we select the locmax method in this study.

We first assume the number of segments N is given. Namely the total number of boundaries is $N+1$. Next, we compute all local maxima and sort them in decreasing order. Finally, the set of Fourier boundaries $\Omega=\{\omega^n\}$, $n=0, 1, \ldots, N$, can be calculated by:

$$\omega^n=\begin{cases}0 & \text{for} \quad n=0,\\ \dfrac{\omega^n+\omega^{n-1}}{2} & \text{for} \quad 1\le n\le N-1\\ \pi & \text{for} \quad n=N.\end{cases} \tag{12}$$

3. ECT-BASED IMPLEMENTATION

To study the distribution of the empirical curvelet coefficients of the desert seismic data, we use a synthetic desert seismic data (Fig. 2a) for experiments. The dominant frequency of the effective signal is 25 Hz. To obtain desert seismic records with low *SNR*, we add simulated random noise of desert seismic to the pure signal. The simulated random noise is modeled by *Li (2016, 2017)*. The *SNR* of the noisy data is −8.74 dB, as shown in Fig. 2b. It shows that the events of the effective signal are submerged in strong random noise. We use the ECT to decompose the noisy desert seismic data into 4 scales and the decomposition directions at scale 1–4 are 1, 4, 4 and 4, respectively. Figure 2c shows the corresponding tilings, it is clear that the Fourier supports for ECT separate the different sub-bands. We also decompose the random noise shown in the Fig. 2b by using the ECT ($N = 4$, $M = 4$). Figure 3a shows the energy spectrum distributions of the above noisy data and its random noise. The energy of the noisy data is greater than that of the random noise at scale 2 direction 4 and their energy is almost the same at the other sub-bands. This suggests that the effective signal can concentrate at one sub-band. For comparison, we also apply the CCT on the noisy data and its random noise. Figure 3b shows the energy spectrum distribution of CCT coefficients. It can be seen that the energy of noisy data is greater than that of random noise at scale 1 and all directions of scale 2. This suggests that the effective signal is distributed to multiple sub-bands. Consequently, empirical curvelet transform can separate the valid signal and random noise more effectively than the conventional curvelet transform.

Based on the above discussion, we divide the empirical curvelet coefficients into two groups for processing. In the first group, the sub-bands belong mainly to noise, therefore, we select a large threshold to remove much noise. The threshold is defined as:

$$Th_{n,m} = \sigma_{n,m}\sqrt{2\log A}\,, \tag{13}$$

where $\sigma_{n,m}$ is the standard deviation of random noise and A is the size of the data. We estimate the standard deviation of random noise from the median of the sub-band coefficients (*Donoho, 1995*).

In the second group, the empirical curvelet coefficients are associated with effective signals. The desert seismic effective signals and random noise share the same sub-band

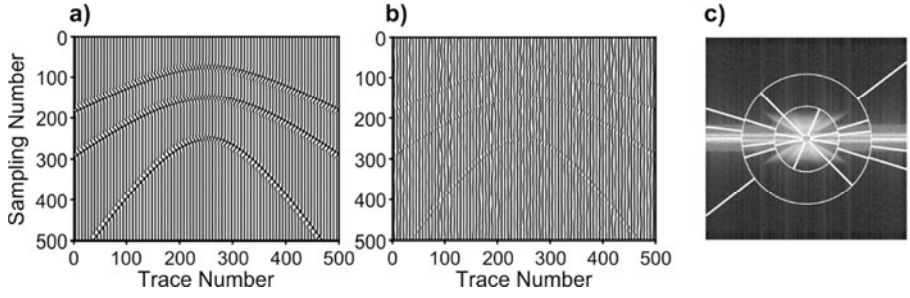

Fig. 2. **a)** Synthetic pure desert seismic signal, **b)** noisy data, **c)** detected Fourier boundaries of the noisy data.

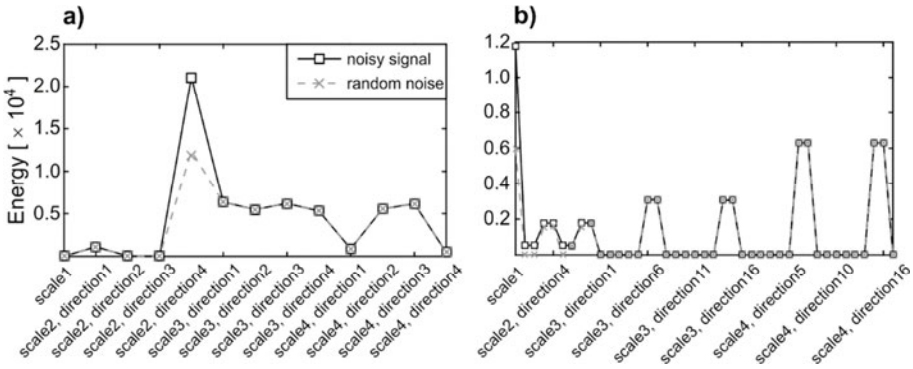

Fig. 3. Energy distribution for: **a)** ECT coefficients, **b)** TCT coefficients.

and the energy of the noise is strong. It is difficult to use simple threshold value for processing the effective signal and noise have similar absolute coefficient magnitudes. To process these coefficients, we adopt a coherence-enhancing diffusion filter (CEDF), which is a boundary preserving filtering method based on thermal diffusion partial differential equation and is suitable for texture image with high *SNR*. Besides, the events of seismic signal have rich line structures, and the seismic data generally exhibits texture features Thus, the CEDF is very applicable for seismic signal processing.

The equation of CEDF is expressed as:

$$\begin{cases} \dfrac{\partial f(x,y,t)}{\partial t} = \operatorname{div}\left(\mathbf{D}\cdot\nabla f\right), \\ f\big|_{t=0} = f_0 \ , \end{cases} \tag{14}$$

where f is the diffusion filter result, f_0 is the original data, t is the diffusion time, and $\mathbf{D}$ is the tensor of the diffusion filter. It is critical to design a proper diffusion tensor $\mathbf{D}$. For seismic data, their gradient directions are perpendicular to the direction of the events. We use the gradient ∇f (*Fehmers and Höcker, 2003*) of seismic signals to form the diffusion tensor $\mathbf{S}(\nabla f)$:

$$\mathbf{S}(\nabla f) = \nabla f \ \nabla f^{\mathrm{T}} . \tag{15}$$

To enhance the robustness of the structure tensor, the gradient structure tensor is processed with small-scale gaussian filtering, and the new structure tensor is obtained as:

$$\mathbf{S}_\eta = G_\eta * \mathbf{S} = \begin{bmatrix} G_\eta * f_x^2 & G_\eta * f_x f_y \\ G_\eta * f_y f_x & G_\eta * f_y^2 \end{bmatrix} = \begin{bmatrix} a & b \\ c & d \end{bmatrix}. \tag{16}$$

The eigenvalue decomposition of $\mathbf{S}_\eta$ can be written as:

$$\mathbf{S}_\eta = \begin{bmatrix} \gamma_1 & \gamma_2 \end{bmatrix} \begin{bmatrix} \lambda_1 & 0 \\ 0 & \lambda_2 \end{bmatrix} \begin{bmatrix} \gamma_1 & \gamma_2 \end{bmatrix}^{\mathrm{T}}, \tag{17}$$

where λ_1, λ_2 are the eigenvalues, and $\begin{bmatrix} \gamma_1 & \gamma_2 \end{bmatrix}$ is a matrix with columns of eigenvectors γ_1 and γ_2.

The eigenvectors of the diffusion tensor **D** are the same as that of the structure tensor $\mathbf{S}_\eta$. If the eigenvalues of **D** are χ_1 and χ_2, the eigenvalue decomposition of **D** can be expressed as:

$$\mathbf{D} = \begin{bmatrix} \gamma_1 & \gamma_2 \end{bmatrix} \begin{bmatrix} \chi_1 & 0 \\ 0 & \chi_2 \end{bmatrix} \begin{bmatrix} \gamma_1 & \gamma_2 \end{bmatrix}^{\mathrm{T}}, \tag{18}$$

χ_1 and χ_2 can be calculated as:

$$\chi_1 = \delta, \quad \chi_2 = \delta + (1-\delta)\exp\left(-\frac{C_{line}}{K}\right), \tag{19}$$

where the diffusivity $\delta \in [0,1]$ represents the filtering intensity of the diffusion filter along each characteristic direction. Eigenvalues of 0 and 1 indicate unfiltered operation and complete filtering operation, respectively. $C_{line} = (\lambda_1 - \lambda_2)/(\lambda_1 + \lambda_2)$ is linear confidence, which is introduced to better reflect the linear characteristics of events, and $K = (\lambda_1 - \lambda_2)^2$. The anisotropic diffusion tensor is substituted into the anisotropic diffusion equation after its construction. Using difference to replace differential, the seismic data achieves anisotropic diffusion, and the denoising result is obtained.

The method of suppression random noise in desert seismic based on the ECT proposed in this study is implemented as follows:

1. The observed noisy desert seismic data are modeled as:

$$f = y + z, \tag{20}$$

   where f is the observed noisy signal, y is the desired signal, and z is the desert seismic random noise. We perform ECT on the noisy signal f, then we can get the following equation:

$$Coe_f(n,m) = \langle f, \Phi \rangle, \tag{21}$$

   where $Coe_f(n,m)$ are the empirical curvelet coefficients at scale n and direction m.
2. Analyzing the energy spectrum distribution of the ECT coefficients, we can divide these coefficients into two groups: the ones associated with noise; the other ones associated with valid signal.

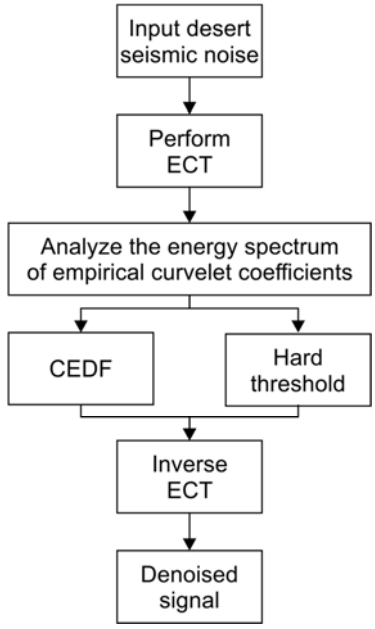

Fig. 4. Workflow of the proposed method.

3. Adopt the hard threshold to the sub-bands that are mainly belonging to noise.
4. Adopt the CEDF to the sub-band associated with valid signals.
5. Perform the inverse ECT to reconstruct the coefficients and then achieve the denoising process.

The workflow of the proposed method is also summarized in Fig. 4.

4. APPLICATION TO DESERT SEISMIC DATA

4.1. Test on synthetic data

To verify the feasibility and effectiveness of our proposed method, we present a synthetic data set as shown in Fig. 5a. This synthetic record contains 7 reflection events with the dominant frequency of 25 Hz, and the sampling number is 500. The noisy data in Fig. 5b is generated by adding synthetic desert seismic noise to the pure signal, giving the *SNR* is −8 dB. These events are almost completely submerged in strong noise. We compare the proposed method with the threshold-based wavelet transform method, the threshold-based TCT method, CEDF method and the CEDF-based TCT method. In the threshold-based method, the thresholding can be obtained by Eq. (13). In the CEDF method, the parameters are selected by judicious tests. The diffusivity parameter δ is 0.006. To ensure that diffusion tensor is positive definite, diffusivity parameter δ must be a small positive number. The value of the iteration time usually belongs to [0.1, 0.25] to make sure the stability of data in the convergence processing. Too short iteration time

causes the number of iterations to increase, which will increase computation time. The number of iterations is between 8 and 12. The results of these methods are shown in Fig. 5c–g. Figure 5c obviously shows that the events in the rectangles are seriously damaged because the wavelet transform is not multi-directional. The effective signals in Fig. 5d are completely recovered, but they are more attenuated compared with other methods.. Besides, some random noise is left, because the traditional curvelet transform

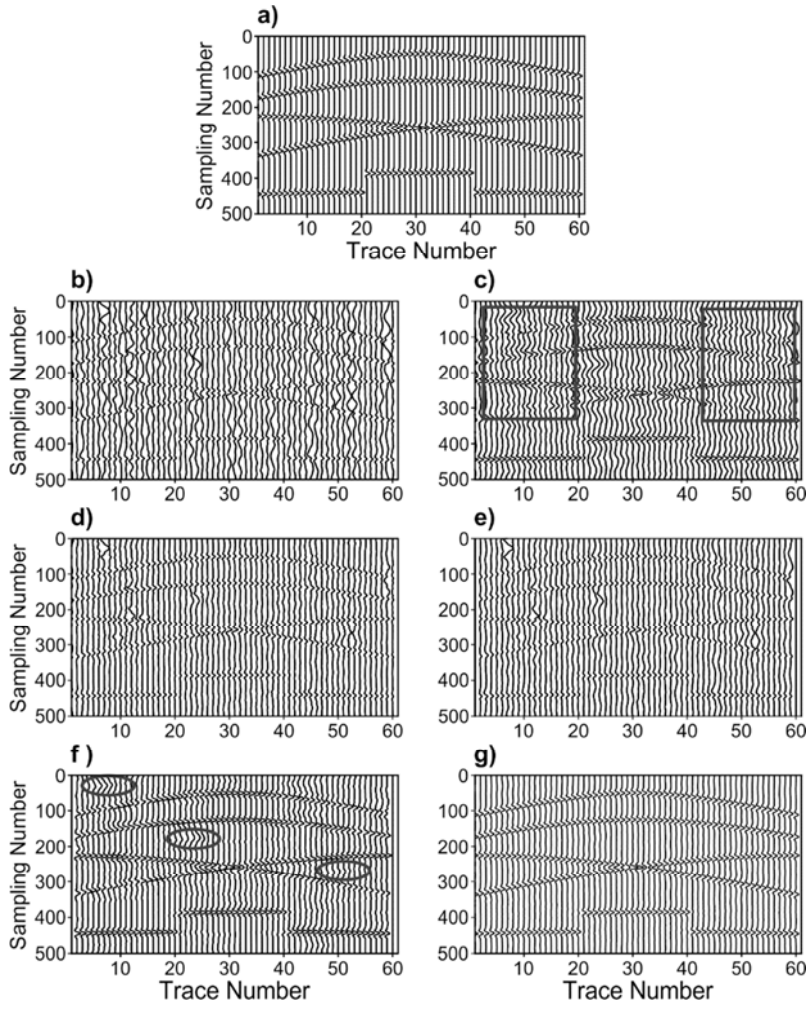

Fig. 5. Comparison of denoising results with synthetic desert seismic data: **a)** synthetic desert seismic data, **b)** synthetic noisy data, **c)** denoised result of wavelet, **d)** denoised result of the threshold-based traditional curvelet transform (TCT) method, **e)** denoised result of the coherence-enhancing diffusion filter (CEDF), **f)** denoised result of CEDF-based TCT, and **g)** denoised result of the proposed method.

is not adaptive to build a filter bank, the effective signal cannot be accurately extracted. Figure 5e is the denoising result by using the CEDF method. The reason of the unsatisfactory denoising effect is that the method cannot perform well under low *SNR*. Figure 5f shows the result of processing with the CEDF-based TCT method. Some strong noise is visible in regions highlighted by ellipses. By contrast, the proposed method shows the best denoising performance. Figure 5g has the cleanest background and the events are more continuous and easier to identify.

To further observe the retention of effective signal components, we extract the 51th trace from the denoised results to compare with the pure signal. Figure 6a–e shows the amplitudes of the signal waveform in time-domain, and Fig. 6f depicts the comparison of frequency-domain. It can be seen that the denoising result of the proposed method is the most similar to the pure signal. We also plot the *f-k* spectra of the pure signal record (Fig. 5a), noisy record (Fig. 5b), and denoising results (Fig. 5c–g) as shown in Fig. 7a–g, respectively. Figure 7a shows the frequency of pure signal ranges from 0 to 75 Hz. Figure 7b shows the frequency ranges from low-frequency to high-frequency. In the red rectangles, we can observe that the random noise in the low-frequency domain overlaps with the effective signals. Figure 7c shows that the valid signal and the noise are all

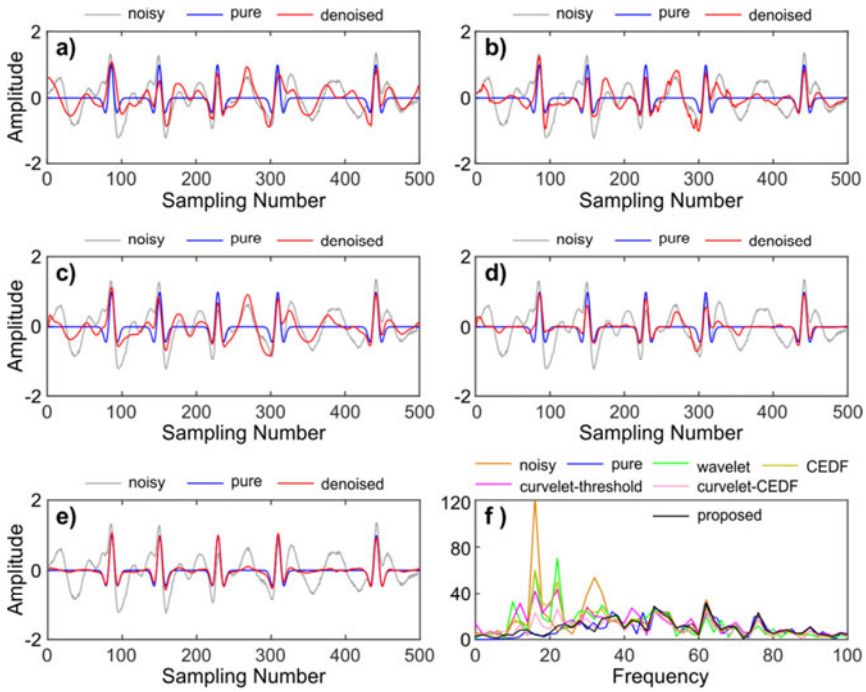

Fig. 6. Comparison of waveform spectra of signal denoised by **a)** the wavelet method, **b)** the threshold-based traditional curvelet transform (TCT) method, **c)** the coherence-enhancing diffusion filter (CEDF) method, **d)** the CEDF-based TCT method, **e)** the proposed method, and **f)** amplitude spectra corresponding to the five methods.

suppressed by using wavelet transform. In the denoising result of traditional curvelet transform (Fig. 7d), some low-frequency noise and high-frequency noise remain in some directions. In the results of CEDF, Fig. 7e, the energy of effective signal is attenuated and some of the low-frequency noise remains. Figure 7f shows the *f-k* spectrum of CEDF-based TCT method denoising result. Though most low-frequency noise is attenuated, some noise which overlaps with signal cannot be removed. The denoising result of the proposed method (Fig. 7g), is the most similar to the pure signal because the basis function of the ECT is adaptive. It could decompose the signal to different sub-bands according to the signal itself.

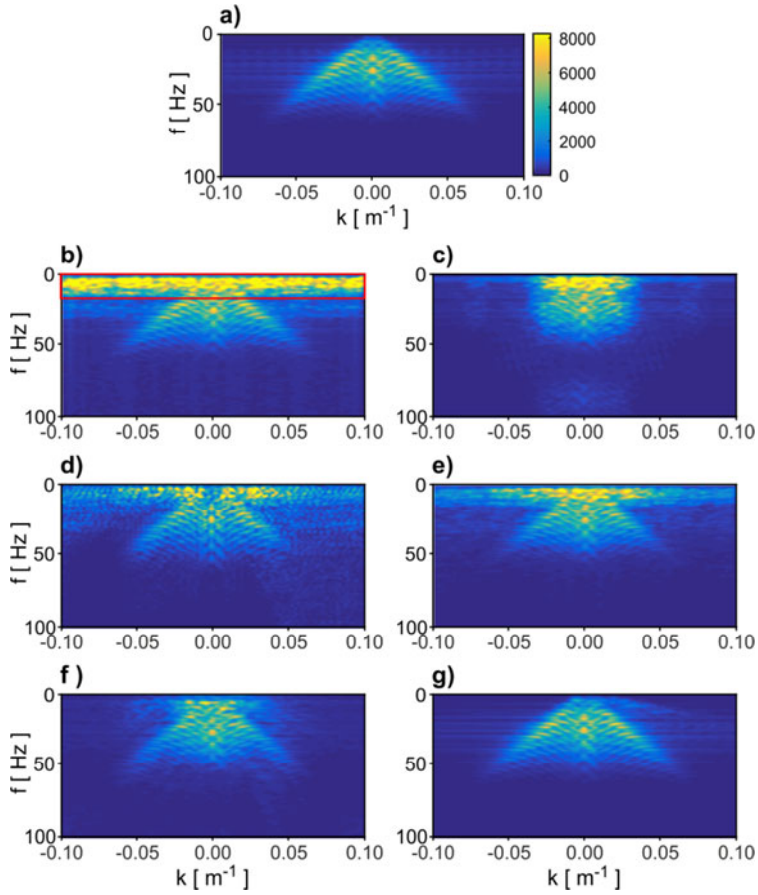

Fig. 7. Frequency-wave number (*f-k*) spectrum of **a)** pure signal, **b)** synthetic noisy signal, and results of **c)** the wavelet method, **d)** the threshold-based traditional curvelet transform (TCT) method, **e)** the coherence-enhancing diffusion filter (CEDF) method, **f)** the CEDF-based TCT method, and **g)** the proposed method.

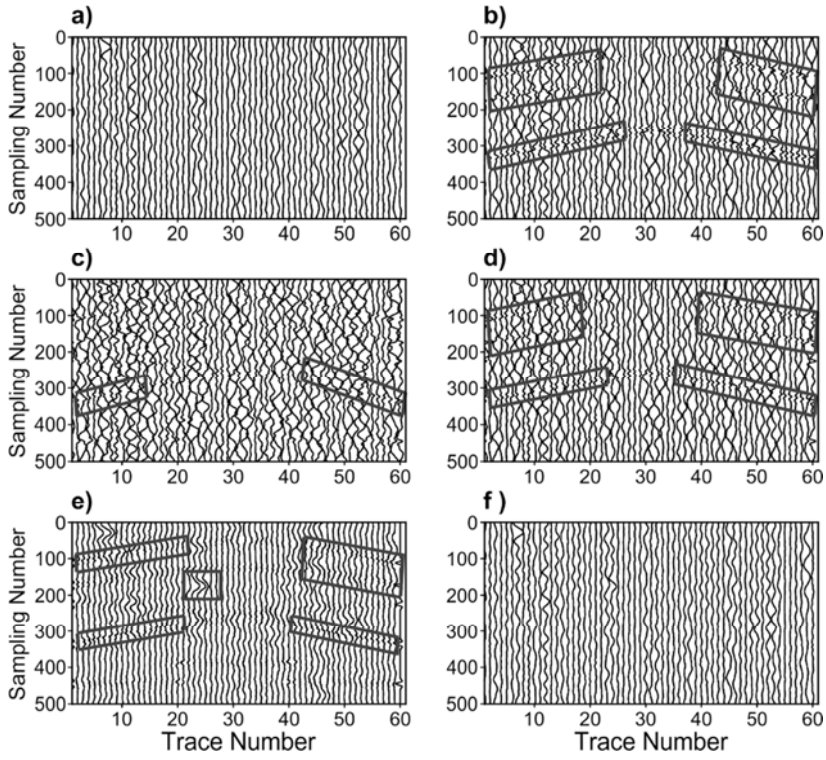

Fig. 8. Differences between **a)** the noisy record, and records recovered by **b)** the wavelet method, **c)** the threshold-based traditional curvelet transform (TCT) method, **d)** the coherence-enhancing diffusion filter (CEDF) method, **e)** the CEDF-based TCT method, and **f)** the proposed method. Quadrangles show obvious residuals of effective signals.

Figure 8a shows the synthetic desert seismic noise, which is added to the Fig. 5b. Figure 8b–f represents the differences between the noisy records and recovered records. It shows that there are obvious residuals of effective signals in Fig. 8b–e (dark-grey quadrangles) and Fig. 8f depicts the closest to the figure of pure noise. Figure 9 gives the *f-k* spectrum of differences. The figure clearly shows that many effective signals left in Fig. 9b–e.

In addition, we quantitatively analyzed the output *SNR* and mean square error (*MSE*) of the methods mentioned above in different *SNR* levels. The results are listed in Table 1 and shown in Fig. 10. These results suggest that denoising result of the method proposed in this paper has the largest *SNR* and smallest *MSE* values.

4.2. Test on field data

Finally, in order to verify the practical application ability of the proposed method, we apply this method on the field records. Figure 11a shows the real seismic records of 130 traces and 2400 points in each trace, which was acquired from a certain area of China. This figure indicates that due to the interference of the random noise, the effective signals

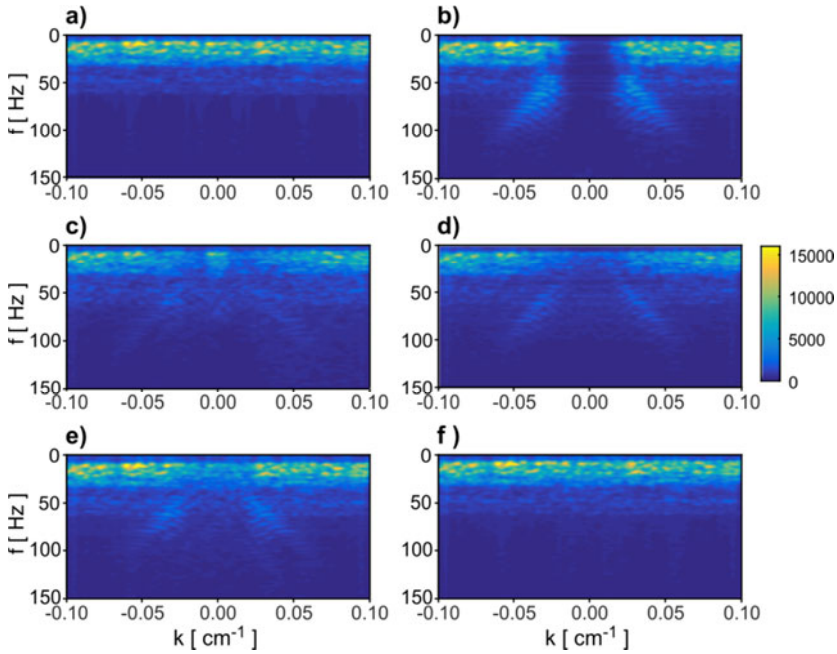

Fig. 9. Frequency-wave number spectra corresponding to the plots shown in Fig. 8.

are submerged in strong noise. Wavelet transform method, threshold-based TCT method, CEDF method, CEDF-based TCT method and the proposed method are applied on this field record, with the results shown in Fig. 11b–f.

It is observed that the backgrounds of the Fig. 11b–f are clearer, indicating that most of the random noise is removed by these methods. Note that the random noise in the rectangles is dominated by high-frequency, and all these five denoising methods can effectively suppress high-frequency random noise. However, the frequency of noise in the elipses is dominated by low-frequency. The method developed in this study obviously outperforms other methods in recovering effective signals. All the reflection events are continuous and clear. Additionally, the suppression of the surface wave in the field record has a good performance.

5. CONCLUSIONS

Low-frequency random noise in desert seismic is non-stationary, non-Gaussian, nonlinear. In addition, it has considerable energy and significantly overlaps with effective signal frequency band, we introduced ECT into desert seismic signal processing in this study. This method effectively extracts different components of desert seismic signals by exploiting the adaptability and sparse properties of the ECT to obtain the empirical curvelet coefficients of different scales and directions. We analysed the energy spectrum

Table 1. Signal-to-noise ratio (*SNR*) and mean square error (*MSE*) of different methods. TCT: traditional curvlet transform, CEDF: coherence-enhancing diffusion filter.

Method	Input *SNR* [dB]	Output *SNR* [dB]	*MSE*
Wavelet	–7.61	–3.56	0.2665
	–3.52	–1.23	0.1556
	–1.59	1.48	0.1024
Threshold-Based TCT	–7.61	–1.76	0.0876
	–3.52	0.37	0.062
	–1.59	1.87	0.031
CEDF	–7.61	–1.31	0.0761
	–3.52	1.43	0.0543
	–1.59	4.78	0.0311
CEDF-Based TCT	–7.61	0.037	0.06
	–3.52	3.95	0.048
	–1.59	7.03	0.025
Proposed	–7.61	4.21	0.0346
	–3.52	7.42	0.0153
	–1.59	9.38	0.0086

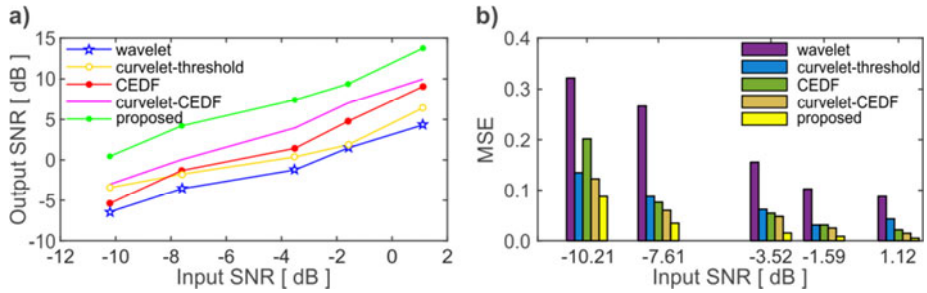

Fig. 10. **a)** Output signal-to-noise ratios (*SNR*) of the five methods for different input *SNR*; **b)** mean square error (*MSE*) of the five methods for different input *SNR*.

distribution of the empirical curvelet coefficients and divided them into different groups. For the first group, which contained fewer effective signals, we used a large threshold to remove the random noise. For the second group, which contained more effective signals, the CEDF was applied to eliminate the random noise. Test on synthetic and field desert seismic data demonstrated that the proposed method achieves good performance in signal preservation and random noise reduction.

Acknowledgments: We thank for the sponsor of the National Natural Science Foundations of China (grant nos. 41730422). We also thank the authors of TCT and ECT for sharing the codes online. Both of these codes are available at *http://www.mathworks.com*.

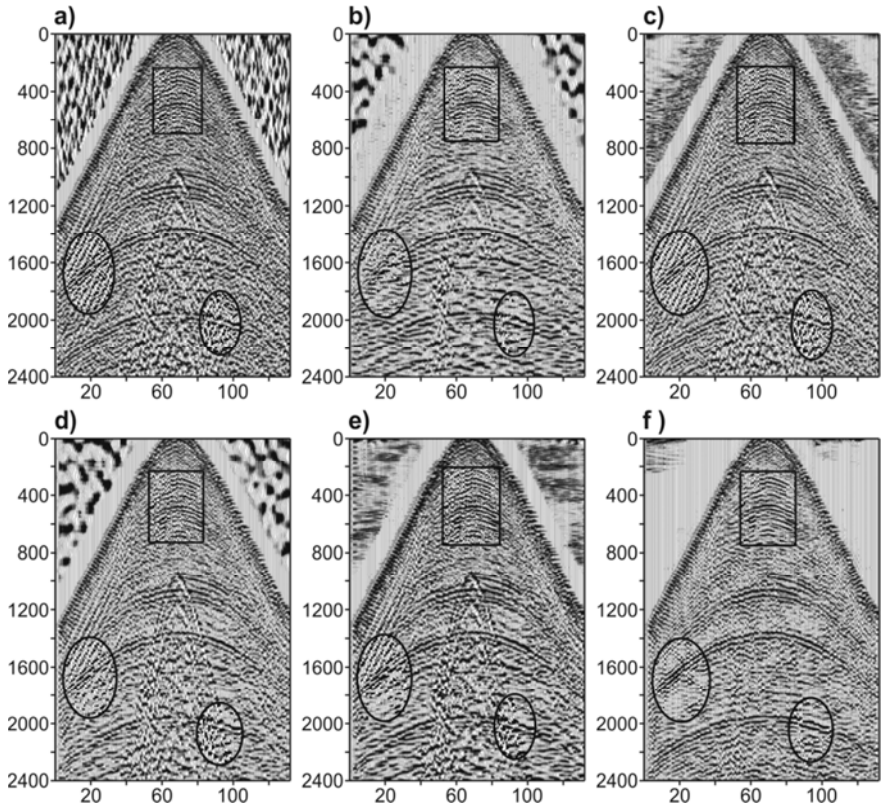

Fig .11. **a)** The real desert seismic data, and results of **b)** the wavelet method, **c)** the threshold-based traditional curvelet transform (TCT) method, **d)** the coherence-enhancing diffusion filter (CEDF) method, **e)** the CEDF-based TCT method, and **f)** the proposed method. Rectangles and elipses show areas with noise dominated by high and low frequency, respectively.

References

Averbuch A., Coifman R.R., Donoho D.L., Elad M. and Israeli M., 2006. Fast and accurate Polar Fourier transform. *Appl. Comput. Harmon. Anal.*, **21**, 145–167.

Averbuch A., Coifman R.R., Donoho D.L., Israeli M. and Shkolnisky Y. 2008. A framework for discrete integral transformations - the pseudo polar Fourier transform. *SIAM J. Sci. Comput.*, **30**, 764–784.

Bonar D. and Sacchi M., 2012. Denoising seismic data using the nonlocal means algorithm. *Geophysics*, **77**, A5–A8.

Bekara M. and van der Baan M., 2009. Random and coherent noise attenuation by empirical mode decomposition. *Geophysics*, **74**, V89–V98.

Candes E., Demant L., Donoho D. and Ying L., 2006. Fast discrete curvelet transform. *Multiscale Model. Simul.*, **5**, 861–899.

Candes E. and Donoho D., 2004. New tight frames of curvelets and optimal representations of objects with piecewise C-2 singularities. *Commun. Pure Appl. Math.*, **57**, 219–266.

Deng X.Y., Yang D. and Yang B., 2008. LS-SVR with variant parameters and its practical applications for seismic prospecting data denoising. *2008 IEEE Int. Symp. Ind. Electron.*, **1-5**, 1060–1063.

Donoho D.L., 1995. Denoising by soft thresholding. *IEEE Trans. Inform. Theory*, **41**, 613–627.

Daubechies I., 1992. *Ten Lectures on Wavelets*. SIAM: Society for Industrial and Applied Mathematics, Philadelphia, PA.

Fehmers G.C. and Höcker C.F.W., 2003. Fast structural interpretation with structure-oriented filtering. *Geophysics*, **68**, 1286–1693.

Fu Y. and Zhang C., 2008. Seismic data denoising based on second wavelet transform. *2008 International Conference on Advanced Computer Theory and Engineering (ICACTE)*. IEEE Computer Society, Washington, D.C., 186–189, DOI: 10.1109/ICACTE.2008.118.

Gong X., Wang S. and Du L., 2018. Seismic data reconstruction using a sparsity-promoting apex shifted hyperbolic radon-curvelet transform. *Stud. Geophys. Geod.*, **62**, 450–465.

Gilles J., Tran G. and Osher S., 2014. 2D empirical transform wavelets, ridgelets and curvelets. *SIAM J. Imaging Sci.*, **7**, 157–186.

Herrmann F. and Verschuur E., 2004. Curvelet-domain multiple elimination with sparseness constraints. *SEG Technical Program Expanded Abstracts*, **12**, 1333–1336.

Hennenfent G., Fenelon L. and Herrmann F., 2010. Nonequispaced curvelet transform for seismic data reconstruction: A sparsity-promoting approach. *Geophysics*, **75**, WB203–WB210.

Jeng Y., Li Y., Chen C. and Chien H., 2009. Adaptive filtering of random noise in near-surface seismic and ground-penetrating radar data. *J. Appl. Geophys.*, **68**, 36–46.

Li G. and Li Y., 2016. Random noise of seismic exploration in desert modeling and its applying in noise attenuation. *Chinese J. Geophys.-Chinese Ed.*, **59**, 682–692 (in Chinese).

Li G., Li Y. and Yang B., 2017. Seismic exploration random noise on land: modeling and application to noise suppression. *IEEE Trans. Geosci. Remote Sensing*, **55**, 4668–4681.

Naghizadeh M., 2012. Seismic data interpolation and denoising in the frequency-wavenumber domain. *Geophysics*, **77**, V71–V80.

Neelamani R., Baumstein A., Gillard D., Hadidi M. and Soroka W., 2008. Coherent and random noise attenuation using the curvelet transform. *The Leading Edge*, **27**, 240–248.

Ristau J. and Moon W., 2001. Adaptive filtering of random noise in 2-D geophysical data. *Geophysics*, **66**, 342–349.

Tian Y., Li Y., Lin H. and Wu N., 2015. Application of GNMF wavelet spectral unmixing in seismic noise suppression. *Chinese J. Geophys.-Chinese Ed.*, **58**, 4568–4575 (in Chinese).

Weickert J. and Scharr H., 2002. A Scheme for coherence-enhancing diffusion filtering with optimized rotation invariance. *J. Vis. Commun. Image Represent.*, **13**, 103–118.

Miao X. and Moon W., 1999. Application of wavelet transform in reflection seismic data analysis. *Geosci. J.*. **9**, 171–179.

Yuan S. and Wang S., 2013. Edge-preserving noise reduction based on Bayesian inversion with directional difference constraints. *J. Geophys. Eng.*, **10**, Art.No. 025001.

Zhong T., Zhang S., Li Y. and Yang B., 2019. Simulation of seismic-prospecting random noise in the desert by a Brownian-motion-based parametric modeling algorithm. *C. R. Geosci.*, **351**, 10–16.

Zhong T., Li Y., Wu N., Nie P. and Yang B., 2015. A study on the stationarity and Gaussianity of the background noise in land seismic prospecting. *Geophysics*, **80**, V67–V82.